JOURNAL OF GEOPHYSICAL RESEARCH, SPACE PHYSICS VOL. 74, NO. 26, DECEMBER 1, 1969

Nonducted Mode of VLF Propagation between Conjugate Hemispheres; Observations on OGO's 2 and 4 of the 'Walking-Trace' Whistler and of Doppler Shifts in Fixed Frequency Transmissions

F. WALTER AND J. J. ANGERAMI

Radioscience Laboratory
Stanford University, Stanford, California 94305

Evidence for nonducted VLF propagation between conjugate hemispheres has been found in records from the broadband VLF receivers aboard the polar satellites OGO 2 (419–1521 km) and OGO 4 (412-908 km). The nonducted signals described here are received in the ionosphere between 47° and 56° invariant latitude. They have never been observed on the ground and include natural whistlers and fixed-frequency signals (10.2–12.5 kHz) from the U. S. Navy Omega transmitters. In a time-frequency spectrogram, these nonducted whistlers appear as *rising tones* with a lower cutoff frequency in the approximate range of 5 to 8 kHz. They have been named 'walking-trace' (WT) whistlers, since a rapid increase in travel time as a function of satellite latitude causes successive examples of the rising trace to 'walk through' other whistlers having equal dispersions and produced by the same sequence of lightning sources. A train of WT whistlers exhibits a nearly constant lower cutoff frequency that is equal to the maximum value of the lower hybrid resonance (LHR) frequency above the satellite and an upper cutoff frequency that decreases with increasing satellite latitude. Reflected waves following a WT whistler can also be received if the LHR frequency below the satellite reaches values greater than above it. Observed spectral shapes of such whistlers resemble a fishhook. Fixed-frequency Omega signals observed by OGO 4 in the hemisphere conjugate to the transmitter frequently have characteristics smiliar to those of the WT whistlers. The Omega signals exhibit two features that are not apparent in the natural whistlers: an enhancement of signal strength and a Doppler shift that increases with latitude and may reach hundreds of hertz. The main characteristics of the above phenomena are explained by tracing nonducted rays between conjugate hemispheres in a model magnetosphere. An equatorial electron concentration profile is derived from the WT whistlers.

1. INTRODUCTION

Satellite studies have revealed a remarkable variety of 'nonducted' whistler phenomena, that is, whistlers whose paths are not confined to field-aligned irregularities in the magnetosphere. Particular types of nonducted whistlers are often observed in relatively limited regions of space and may exhibit unusual dispersion properties that vary rapidly with observing position. Such effects invite attempts at analysis by ray tracing. For example the magnetospherically reflected (MR) whistler has been explained qualitatively by *Smith and Angerami* [1968], based on *Kimura*'s [1966] ray tracing program.

The purpose of the present paper is to describe and interpret a new whistler phenomenon identified in midlatitude (~50°) spectrographic records from the VLF experiment aboard the low-altitude polar satellites OGO 2 (419–1521 km) and OGO 4 (412–908 km). These whistlers, first called to our attention by John Katsufrakis of our laboratory, have been named 'walking-trace' (WT) whistlers, for reasons explained below. In contrast to the MR whistler, whose path reaches the equatorial region and then oscillates back and forth across the equator, the WT whistler crosses the equator and then continues downward into the conjugate ionosphere. The WT whistler and its counterpart in man-made VLF signals presents a remarkable variety of effects, including limited latitude range of observation, rapid variation in travel time with position, upper and lower intensity cutoffs, focusing, and Doppler shifts. Ray tracing analysis, applied for the first time to a complex nonducted whistler propagating between conjugate ionospheres, has been successful in predicting nearly all of the observed effects. (Sev-

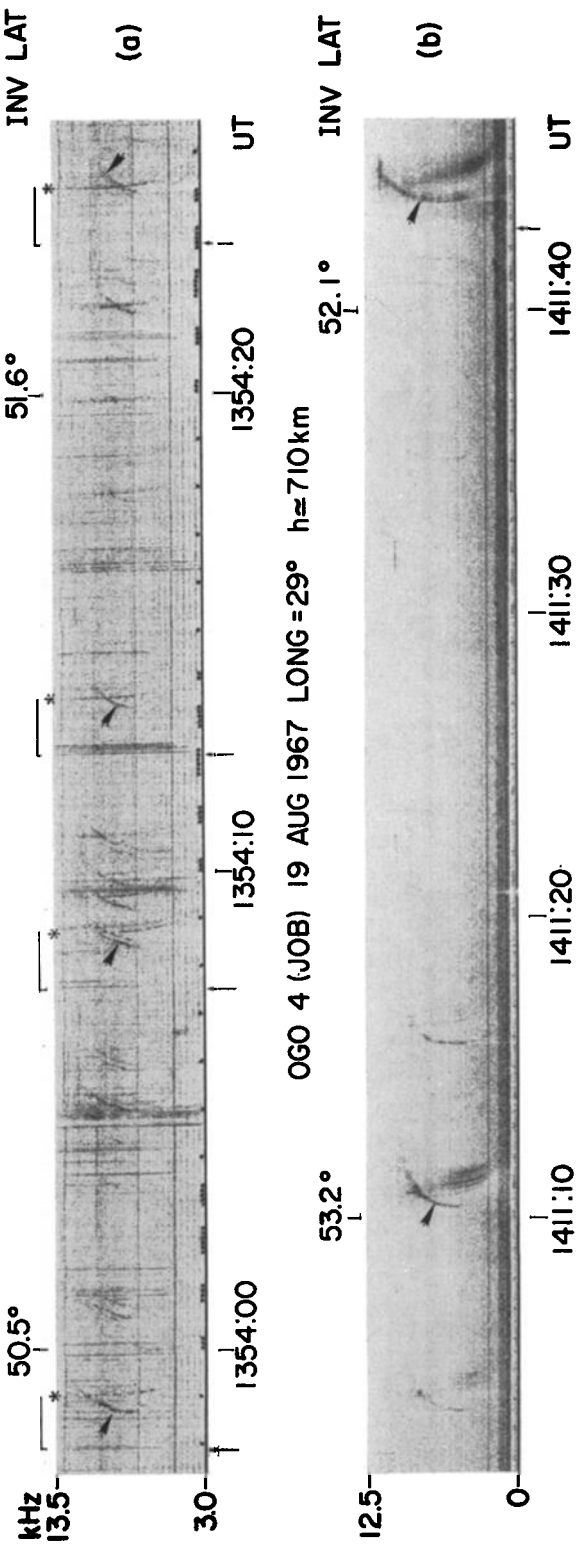

Fig. 1. OGO 4 records of frequency versus time and invariant latitude illustrating several features of 'walking trace' (WT) whistlers. In panel (a) four independent events are labeled, each consisting of three related components, (1) the impulsive signal propagating upward through the nearly ionosphere (vertical arrow at the bottom), (2) a falling tone whistler (asterisk), and (3) the WT whistler (heavy arrow). In panel (b) multicomponent falling tone whistlers are associated with the WT components indicated by the heavy arrows. Fixed-frequency signals at 10.2 and 11⅛ kHz from an Omega transmitter in the conjugate region (Aldra, Norway) appear after 14h11m20s as latitude decreases. These signals are interpreted as following the ray path of the WT whistlers. The measured travel time of the last Omega signal was used to locate the time of origin of the last whistler event (vertical arrow at bottom). A band of hiss appears below 1.7 kHz. The horizontal lines are interference at multiples of 2461 Hz.

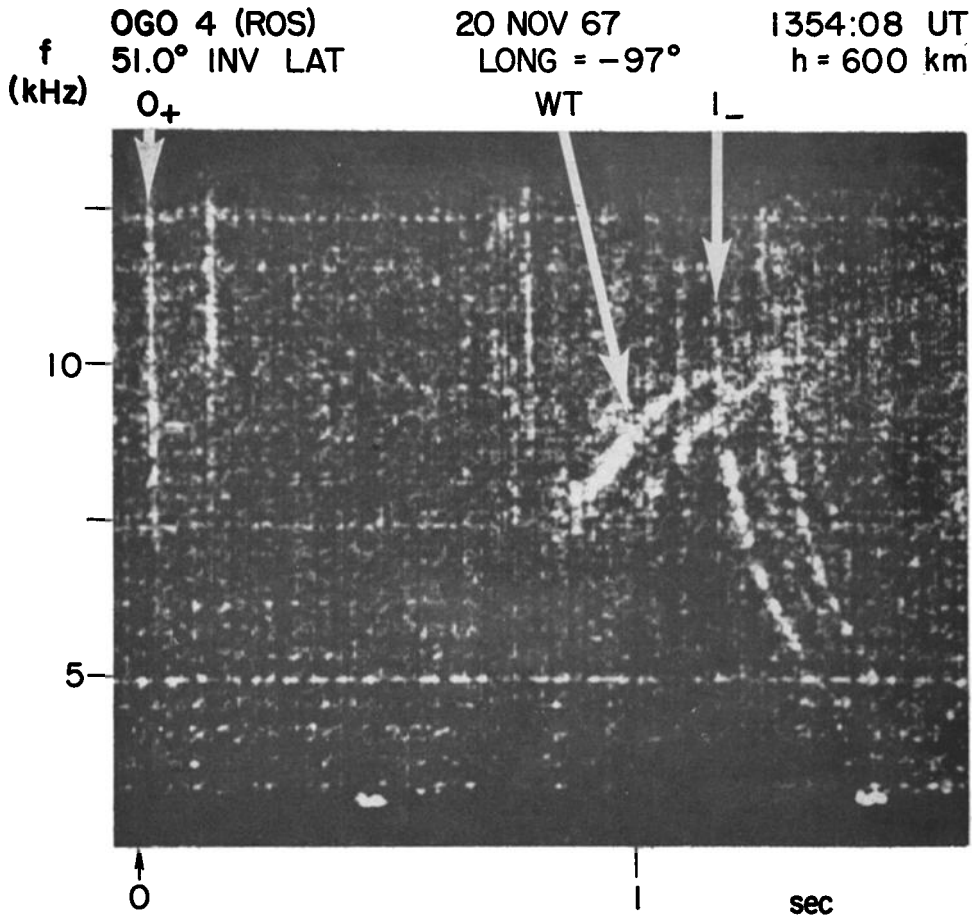

Fig. 2. Expanded frequency-time spectrogram of the second WT whistler event shown in Figure 1*a*. There are actually two independent events spaced by ~0.1 sec. The time origin indicates the time of occurrence of the lightning discharge that produced the indicated whistler components. The horizontal lines are interference at multiples of 2461 Hz.

eral of the effects were only recognized as part of the WT phenomenon after ray tracings were made.)

The next section contains a brief description of the observations. Following this is a description of the ray tracing analysis and a discussion of the physical factors influencing the various WT whistler properties. Later sections are devoted to details of the observations.

2. Description of the WT Whistler

On frequency-time records from satellites, WT whistlers appear as rising tones whose travel time increases rapidly with increasing satellite latitude. The main features of the WT whistler are illustrated on an OGO-4 record in Figure 1*a*. Frequency in kHz is displayed versus UT and invariant latitude on a northbound pass over Rosman, North Carolina. Heavy arrows identify four WT whistlers. Typical features are the relatively constant lower cutoff frequency and an upper cutoff frequency that decreases with increasing satellite latitude. The second event is shown with an expanded time scale in Figure 2.

For each of the WT whistlers identified by a heavy arrow in Figure 1*a*, a vertical arrow in the lower margin identifies a corresponding nearly impulsive whistler. It propagates on the short, so-called 'fractional hop' or 0_+ path up

through the nearby ionosphere to the satellite. A horizontal bar and asterisk in the upper margin identify still a third whistler component produced by the same lightning source. This whistler propagates on a long, so-called one-hop or 1_ path between conjugate hemispheres. Although nonducted, its path is topologically different from that of the WT whistler because the wave normals are small, as a result of horizontal gradients in the ionosphere [*Scarabucci et al.*, 1969]. Within a measurement uncertainty of less than 20 msec, the dispersion of the 1_ whistlers does not change throughout the record, whereas the travel time of the WT events increases significantly during the same interval of time. This is evidenced by the fact that the WT and the 1_ whistler cross at a point that moves to lower frequencies with increasing latitude. Hence, it appears that the WT 'walks through' the 1_ whistler, giving rise to the name 'walking-trace' (WT) whistler.

When ray tracings were developed to analyze whistlers of the type shown in Figures 1 and 2, the analysis indicated that fixed-frequency sig-

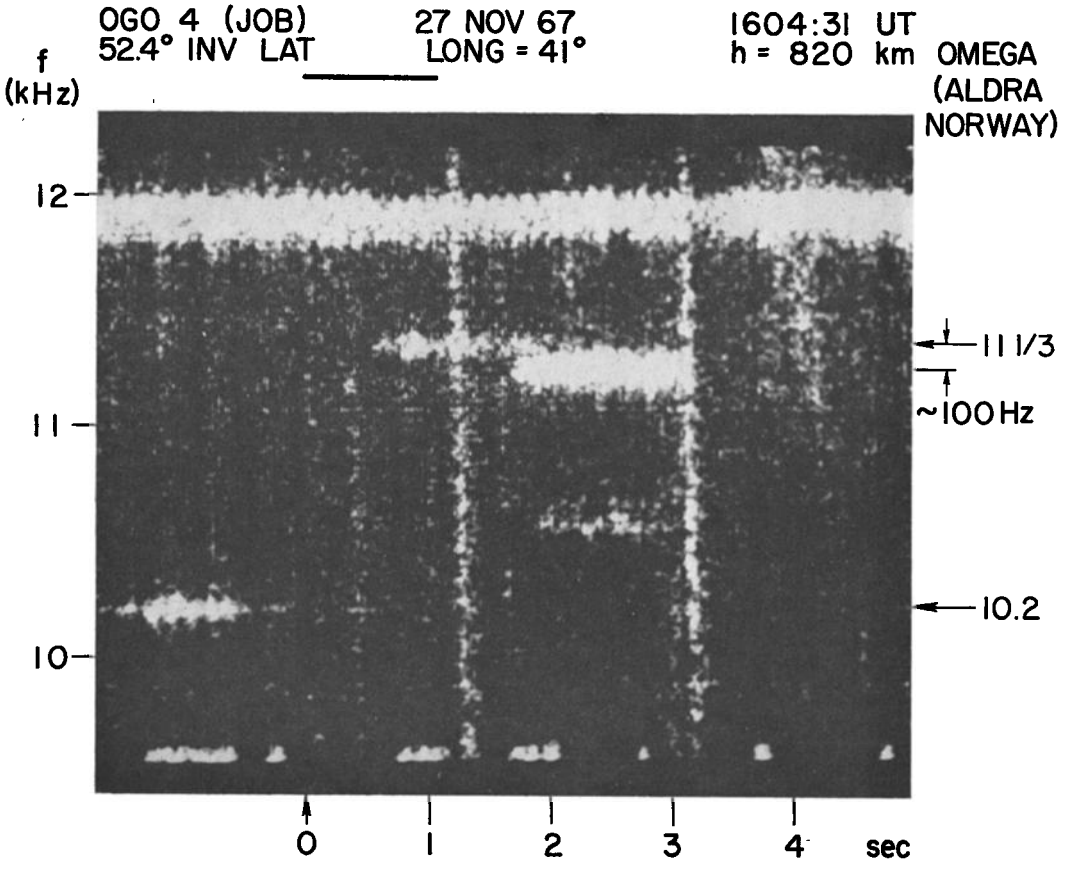

Fig. 3. OGO 4 frequency-time spectrogram illustrating an ~100 Hz Doppler shift in nonducted fixed-frequency signals from an Omega transmitter in the conjugate region (Aldra, Norway). A transmitted pulse at 11⅓ kHz is represented above the record by the dash beginning at $t = 0$. This pulse is received twice by the satellite. The first signal, presenting no Doppler effect, appears at 11⅓ kHz, $t \sim 0.6$ sec. The second is shown by a strong dash at $t \sim 1.8$ sec with a negative Doppler shift of about 100 Hz. The strong continuous signal near 11.9 kHz is transmission from an unidentified VLF station. The nearly vertical lines are whistlers. Dots at the bottom of the record are time marks generated at the telemetry station. An Omega signal at 10.2 kHz appears near the left margin.

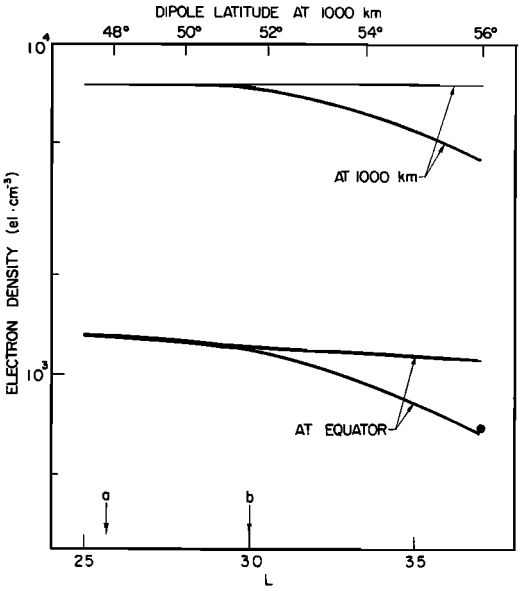

Fig. 4. Models of the electron concentration variation at 1000 km as a function of dipole latitude (top) and at the equator as a function of L values (bottom). The heavy lines represent the basic model used in this paper, the thin lines a constant density model used for comparison. The portion between points a and b indicates the range of equatorial L values crossed by the rays that produced the WT whistlers shown in Figure 13. A dot shows the equatorial electron concentration measured using a nose whistler observed on OGO 4 a few minutes after the events shown in Figure 1a were recorded.

nals propagating in the 'WT mode' should exhibit both focusing and Doppler shift effects. Such effects were found in the data, and now may be understood as a natural part of the WT phenomenon.

Examples of focusing and Doppler shifts appear in receptions by OGO 4 of fixed-frequency signals from the U. S. Navy Omega navigation stations. These signals may exhibit anomalously large intensities and also Doppler shifts that reach hundreds of Hertz. A typical example is illustrated in the frequency-time spectrogram of Figure 3, recorded by OGO 4 near Johannesburg, South Africa. A pulse at 11⅓ kHz transmitted by the Omega station at Aldra, Norway (66°25′N, 13°09′E) is represented in the upper margin of the record by a line with duration 1.1 sec starting at $t = 0$. This pulse is received twice by the satellite. The first signal begins at 11⅓ kHz in the center of the record, near $t = 0.6$ sec. (This signal and the 1-whistlers of Figure 1a are believed to follow analogous paths, differing topologically from those of the WT mode.) A second, stronger pulse appears just below and to the right, starting at $t = 1.8$ sec. This signal exhibits a negative Doppler shift of about 100 Hz, and is interpreted as propagating to the satellite in the same kind of nonducted mode as the WT whistlers of Figures 1 and 2. (An Omega signal at 10.2 kHz appears near the left margin of the record. Signals in the WT mode at this frequency are not seen here, but were observed at higher latitudes—see Figure 12.) A later section presents some relatively complex examples of the data, including simultaneous occurrence in the WT mode of whistlers and fixed-frequency signals.

3. A Ray-Tracing Interpretation of the WT Whistler

Whistlers with the characteristics described above were reproduced by tracing nonducted ray paths from one hemisphere to the conjugate region. Ray tracings in a cold plasma, with the effects of ions included, were made with a FORTRAN H program written by one of the

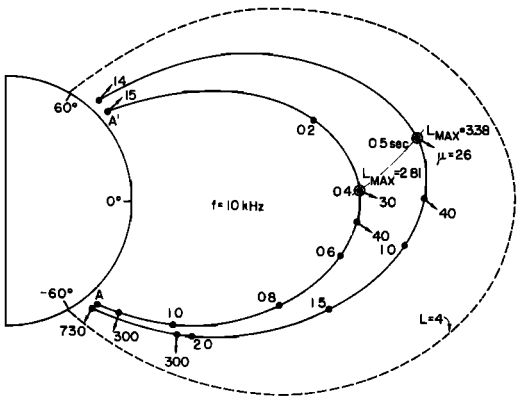

Fig. 5a. Ray paths calculated for wave packets at 10 kHz starting with vertical wave normals at 500 km and invariant latitudes of 44.3° (point A') and 49.9°. A dipole field line at $L = 4$ is shown for reference. Arrows indicate the wave normal directions, and the accompanying values of the phase refractive index μ are indicated. Travel times calculated from the starting points at 500 km are indicated at several points along the rays. The thin line shows the locus of the L_{max}.

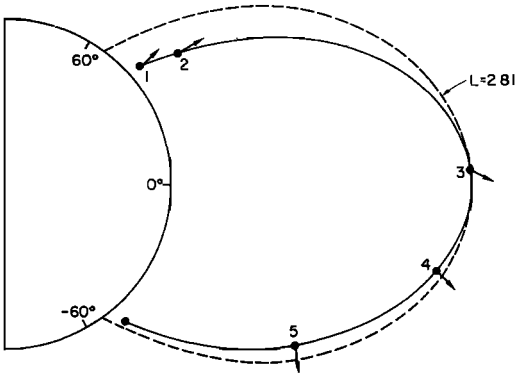

Fig. 5b. Sketch of the inner ray path from Figure 5a, showing the dipole field line through the maximum L along the path.

authors [*Walter*, 1969]. The program is based on the differential equations developed by *Haselgrove* [1954], and it is similar to that used by *Kimura* [1966]. The model magnetosphere was represented by a dipole magnetic field and isothermal diffusive-equilibrium distribution [*Angerami and Thomas*, 1964] of electrons and ions along the field lines at 3000°K. An ion population of 90% O^+ and 10% H^+ was assumed at 1000 km. The model of the variation of electron concentration at (1) 1000 km as a function of latitude and at (2) the equator as a function of L value is shown in Figure 4 by the heavy lines. The thin lines, shown for comparison, correspond to a constant density model at 1000 km. (The ray tracing analysis described below predicts that certain features of the WT mode are highly sensitive to the indicated type of change in model.)

Figure 5a illustrates nonducted ray paths for waves at 10 kHz starting in the northern hemisphere at two different invariant latitudes (44.3° and 49.9°) with vertical wave normals at an altitude of 500 km. A dipole field line at $L = 4$ is shown for reference. Cumulative travel time along the paths (in sec) is indicated at the series of dots. The direction of the wave normal is indicated by arrows at several points, and at the arrows the value of the refractive index μ is marked. Thus the path beginning with vertical wave normal at A' has an initial μ of 15. To clarify Figure 5a, Figure 5b shows the single ray path $A' - A$ and also the dipole field line of maximum L value along the path (dashed curve). Figure 5c presents five refractive index diagrams (not strictly to scale) to illustrate wave normal and ray direction at the points (1) through (5) of Figure 5b. At point (1), the wave normal is vertical, and the ray, whose direction is normal to the refractive index surface, points outward toward higher L values. The wave normal is initially pulled away from the vertical toward $\mathbf{B}_0$ by the effect of the horizontal gradient in the magnetic field. The vertical gradient of electron concentration then becomes a controlling factor, causing further tilting of the wave normal toward $\mathbf{B}_0$. At some point (2) ψ reaches a minimum, beyond which it increases under the influence of the curvature of the magnetic field. Meanwhile, the ray continues to point outward, but at progressively smaller

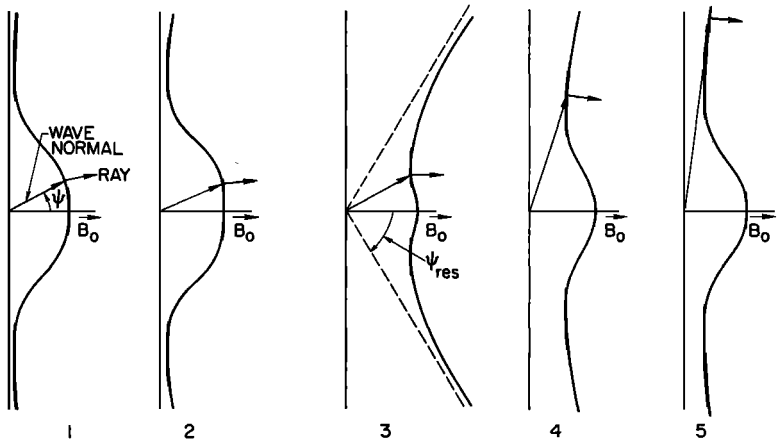

Fig. 5c. Five refractive index diagrams (not strictly to scale) indicating the wave normal and ray directions of four representative points along the ray path of Figure 5b.

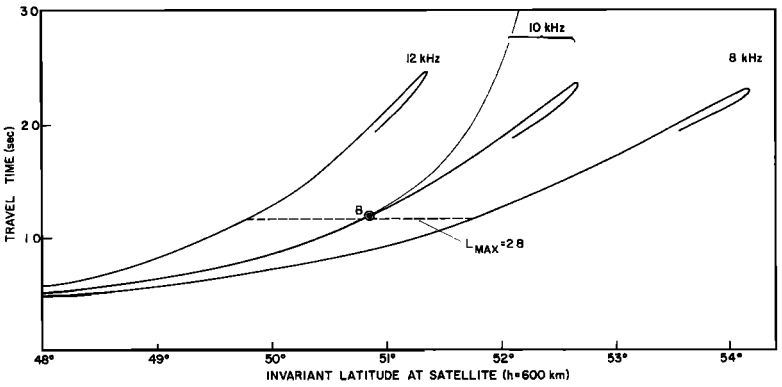

Fig. 6*a*.

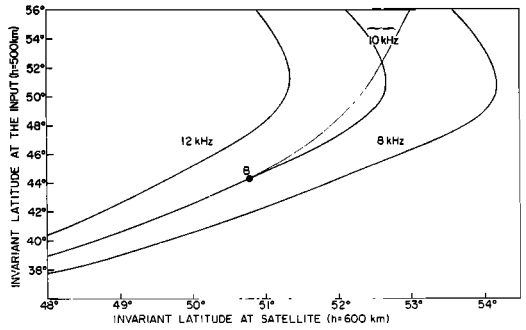

Fig. 6*b*.

Figures 6*a* and *b* show plots of calculated travel time (*a*) and invariant input latitude at 500 km (*b*) versus observing latitude at 600 km in the conjugate hemisphere. For illustration, point *B* corresponds to the ray path $A' - A$ of Figure 5*a*. The dashed line in (*a*) indicates the outermost *L* shell reached by the ray paths. The thin lines correspond to the model with constant density at 1000 km shown in Figure 4.

angles until it is oriented parallel to the magnetic field (3). This is the point of L_{max}, since from here on the ray direction is inward with respect to $\mathbf{B}_0$.

Between (3) and (4) ψ continues to increase under the influences of the curvature and the radial gradient of the magnetic field. The value of μ now increases rapidly, as shown by the increase from $\mu = 30$ to $\mu = 40$ on path $A' - A$ in Figure 5*a*. At point (4), ψ is close to the resonance angle ψ_{res}, and the ray path is strongly dependent on the configuration of the magnetic field. At point (5), the resonance angle and the associated angle ψ have increased until the ray is approximately parallel to $\mathbf{B}_0$. Hence the ray follows closely a geomagnetic field line for the last several thousand km.

Another view of the ray tracing results is shown in Figure 6*a* where travel time through the magnetosphere to a satellite at 600 km is plotted as a function of the invariant latitude of the arrival point, with the wave frequency used as a parameter. (The thin line represents the constant-density-at-1000-km model of Figure 4.) The coordinates of the point *B*, for instance, are the time of propagation from A' to A (cf. Figure 5*a*) and the invariant latitude of point A. The dashed lines in Figure 6*a* indicate the outermost *L* shell reached by each ray (for point *B*, $L_{max} = 2.81$). Figure 6*b* shows a corresponding plot of input latitude versus observing latitude. (Wave normals are assumed vertical at the input.) Point *B*, corresponding to path $A' - A$ of Figure 5*a*, represents $\theta_{IN} = 44.31°$, $\theta_{OBSERVED} = 50.78°$. The input latitudes in Figures 6*a* and 6*b* were limited to 56°. (The behavior of rays starting above ~51° is very sensitive to details of the horizontal gradients in the ionosphere and is under investigation.)

Figures 6*a* and *b* may be used to predict a number of features of the WT mode. At a fixed satellite latitude, for example, travel time increases with frequency in the general manner illustrated by the data of Figure 1. For an observer at 51°, the calculated travel time at 8 kHz is ~0.8 sec and increases to ~2.0 sec

for $f = 12$ kHz. For a fixed frequency, say $f = 10$ kHz, travel time increases with increasing starting and observing latitude (see also Figure 5*a*), ranging from near 0.8 sec at 50° observing latitude to ~2.0 sec at 52°. Note that over this 2° change in endpoint latitude, the initial latitude changes by ~6°, from ~42° to ~48°.

Several features of the data will now be discussed in terms of the predictions of Figures 5 and 6.

Lower cutoff frequency effects in the WT mode. The downcoming rays in Figure 5 exhibit wave normals that are nearly, but not quite, transverse to the geomagnetic field. This condition continues on downward as long as the refractive index surface is open, that is, as long as the wave frequency is above the local lower hybrid resonance (LHR) frequency. If the LHR frequency reaches and then exceeds the wave frequency, the refractive index surface becomes closed and shrinks in size. This condition, combined with the large refractive indices generally encountered in the WT mode below a few thousand kilometers, leads to reflection as in the case of MR whistlers [*Smith and Angerami*, 1968]. Thus a satellite will not receive waves in the WT mode at frequencies below the maximum value of the LHR frequency above the spacecraft. If this maximum value does not change rapidly over a few degrees in latitude, WT whistlers observed on a single satellite pass should exhibit a relatively constant lower cutoff frequency. This is in fact the case, as Figure 1*a* illustrates.

Variation of the LHR frequency with height at an invariant latitude of 51° is shown in Figure 7 for the model magnetosphere used. The LHR frequency has two maxima, a lower one produced by the density peak at the *F* layer and an upper one by the transition from heavy ions (O^+) to light ions (H^+). In this work the term 'maximum LHR frequency' will refer to the upper maximum. The curve in Figure 7 implies that WT whistlers observed by a satellite below 2000 km altitude will have a lower cutoff at 7.5 kHz (compare with data of Figure 1*a* and Figure 2, showing a lower cutoff at about 7.4 kHz).

Figure 7 implies that a satellite situated above the level of the maximum LHR frequency could receive both downcoming and reflected upgoing waves within a frequency range between the local and the maximum LHR below the satellite. A limited number of WT whistlers exhibiting this double component feature have been observed. An example, received by OGO 4 at an altitude of 792 km in the vicinity of Byrd Station, Antarctica, is shown in Figure 8. The WT whistler, indicated by the arrow, resembles a fishhook and is seen in a frequency range of 6 to 8.3 kHz. The portion between 6 and 7 kHz is observed again about 70 msec later, suggesting a reflection of these waves below the satellite in the manner proposed above.

WT whistlers of this kind yield information both on the value of the LHR at the satellite (minimum frequency reflected, 6 kHz in Figure 8) and on a lower bound for the maximum LHR below it (maximum frequency reflected,

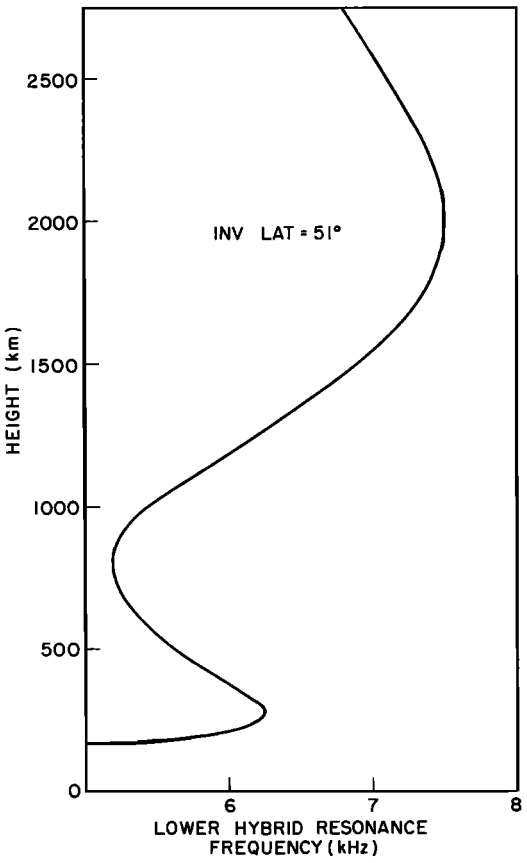

Fig. 7. Behavior of the lower hybrid resonance (LHR) frequency with height at 51° invariant dipole latitude, for the model magnetosphere used.

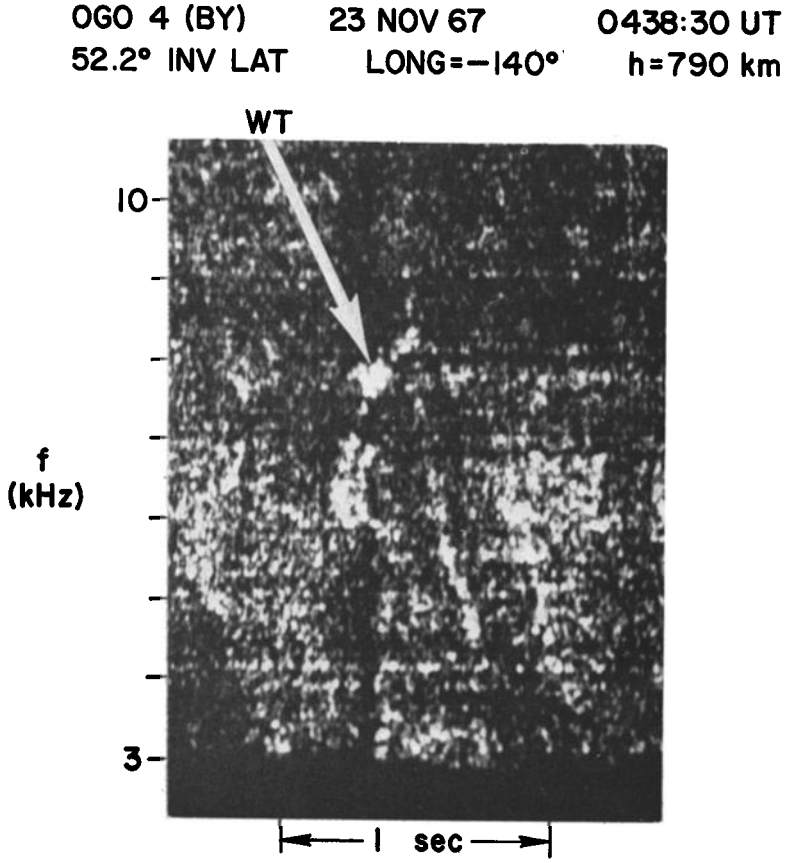

Fig. 8. Frequency-time spectrogram of a walking-trace (WT) whistler (arrow) exhibiting two closely spaced components between the lower cutoff at 6 and 7 kHz. The descending tone following the WT whistler was produced by the same lightning discharge.

7 kHz in Figure 8). The effect is similar to that producing the Nu whistler observed on the higher-altitude satellite OGO 1 [*Smith and Angerami*, 1968]. Reflection at the LHR frequency has also been studied by *Smith et al.* [1966] and *Storey and Cerisier* [1968] to explain bands of noise observed on the electric antenna of Alouette 1 near the LHR frequency [*Barrington and Belrose*, 1963; *Brice and Smith*, 1965].

Upper cutoff frequency effects in the WT mode. Figures 6*a* and *b* predict an upper cutoff frequency in WT whistlers, in the sense that rays at a given frequency will be confined within some upper limiting latitude. This effect can be appreciated from a comparison of the two ray paths for $f = 10$ kHz of Figure 5*a*. As input latitude increases, the value of L_{max} increases. However, the latitude of the point L_{max} also increases (along the thin line). This permits a considerable increase in length of the path segment over which the ray is tilted inward from $\mathbf{B}_0$ (segment corresponding to (4)–(5) of Figure 5*b*). Thus the increasing 'asymmetry' about the equator tends to compensate for the increase in L_{max}, and ray paths tend to cluster at a single value of L_{final}.

Variations in the model of electron concentration cause the locus of L_{max} in Figure 5*a* to be shifted or distorted. There are then appreciable changes in the predicted high frequency behavior in the WT mode. For example, in Figure 6*b* the solid curves based on the model exhibiting a horizontal density gradient (Figure 4) reach a maximum latitude of 52.7° for a wave at $f = 10$ kHz starting at 50.8°. Rays starting at higher initial latitudes cross over the

other paths and arrive at latitudes less than 52.7°, with lower travel times (see Figure 6*a*). However, the thin line in the same figure (corresponding to constant density at 1000 km) extends above 52.7°.

Both density models lead to predictions of a decrease in upper limiting frequency with increasing observing latitude. Clear upper-cutoff effects of this kind are shown in Figure 10, middle of the upper panel. Additional comments on upper-cutoff effects are given below in the section on comparison of calculated and observed spectra.

Latitudinal limits of observation of the WT mode. WT mode propagation was identified in whistlers and/or Omega transmission on about 100 of 300 OGO 2 and OGO 4 passes representing the period August 1967–February 1968. WT-mode effects were observed only in data from the range of invariant latitudes of 47° to 56°. One obvious mechanism for the high-latitude limit is a bandwidth effect, wherein the frequency range of the WT whistler decreases with increasing observing latitude until the upper and lower cutoff frequencies coincide. This tendency is illustrated in the upper panel of Figure 10, where the upper cutoff falls relatively smoothly from 13 kHz near 51° to about 5 kHz near 56°. The lower cutoff effects are not well-defined here, being illustrated more clearly in Figure 1.

The high-latitude limiting-bandwidth effect is shown qualitatively in Figure 6*a*, where the observable bandwidth as a function of latitude is that region of plotted frequencies above the $f = 8$ kHz line (assuming that a $f_{LHR(max)} \sim 8$ kHz). For example, at 51.37° the bandwith is 4 kHz.

At low latitudes, observation of the WT trace is not in general limited by accessibility but rather by the reduction in the range of observable travel times. For example, Figures 6*a* shows that at low observing latitudes, say near 49°, the difference in travel time with increasing frequency is small; hence the characteristic rising form of Figure 1 is not observed.

Local time of occurrence of the WT mode of propagation. It was noted above (cf. Figure 6*a*) that the high-frequency, large-dispersion range of the WT whistler is highly sensitive to the electron concentration distribution in the upper ionosphere and magnetosphere. As gradients of the type shown by the solid curve of Figure 4 are extended to lower L values, the effect in Figure 6 is to cause still larger departures from the behavior of the thin lines and to cause the double values condition to arise at much lower travel times and input latitudes. The result is a prediction that the WT mode should not occur under daytime conditions that involve large-scale horizontal gradients in the ionosphere of the type shown by satellite experimenters such as *Brace et al.* [1967].

This prediction was verified by an analysis of VLF data from more than 300 real time passes of OGO 2 and OGO 4 for the period August 1967 to February 1968. The telemetry stations used were Byrd Station, Antarctica; Santiago and Quito, South America; Rosman, North Carolina; Johannesburg and Madagascar, South Africa. WT modes were observed only in data from Byrd, Johannesburg, Rosman and Madagascar, and as noted above, only in the range of invariant latitudes 47° to 56°.

Figure 9 illustrates the tendency for WT mode activity to be confined to nighttime hours. All data from all passages of OGO 4 over Johannesburg during the month of September 1967 are represented. Filled symbols indicate

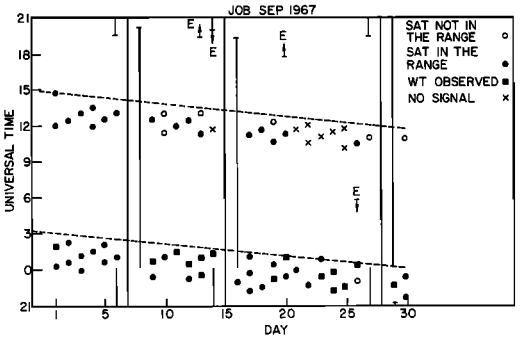

Fig. 9. OGO 4 data showing a concentration of WT-mode activity on the nightside of the earth. Passes over Johannesburg (JOB) for the month of September 1967 are represented in coordinates of universal time versus day of the month. The dashed line indicates the approximate local time of the passes. Symbols used to represent the data are shown at the upper right corner of the figure (see text for details). Periods during which the VLF experiment was turned off are indicated by vertical lines. The periods of operation in an electric-antenna mode are indicated by *E* and arrows.

that the satellite was in the invariant-latitude range of WT propagation, and squares indicate the presence of WT mode effects. The periods when the VLF receiver was connected with an electric antenna are indicated by the arrows labeled *E*. The solid vertical line indicates periods when the VLF experiment was turned off. Crosses indicate those passes on which the unbalanced electric antenna of OGO 4 did not operate properly due to strong interference in sunlight (J. Katsufrakis, personal communication). The approximate local times at the satellite are given by the dashed lines.

The figure indicates that the WT mode was observed only during local nighttime hours and that it was observed both by electric and magnetic antennas. The latter result is expected from the interpretation of the WT mode as an essentially electromagnetic phenomenon.

The occurrence of the WT mode as a function of magnetic activity. There is as yet no evident dependence of the occurrence of WT whistlers on magnetic activity, at least within a range from very quiet conditions to conditions of moderate disturbance. For example, referring to Figure 9 and the observations during the month of September 1967 near Johannesburg, of the 15 passes involving WT mode observations, 10 were such that $\Sigma\ Kp$ for the preceding day was <20, 5 involved $\Sigma\ Kp > 20$.

Simultaneous occurrence of the WT mode and of falling tone whistlers. The simultaneous occurrence of the rapidly varying walking-trace and the slowly varying falling-tone (1_-) whistlers of Figure 1 is apparently due to a condition in which there are horizontal gradients in the ionosphere. It was first thought that the constant-dispersion whistlers might be scattering from a duct. However recent research by R. Scarabucci (personal communication) suggests that they are nonducted but propagate at relatively small wave-normal angles, as a result of horizontal density gradients in portions of the magnetosphere. The presence of these gradients also limits the occurrence of WT whistlers in latitude, as shown in Figure 6.

4. Focusing and Doppler Shifts in the WT Mode; Observations of Omega Fixed-Frequency Transmissions

Focusing and related effects in a case study involving whistlers and fixed-frequency signals. Focusing effects are a natural consequence of the convergence of ray paths discussed above in connection with Figure 5*a*. Figure 6*b*, for example, predicts that rays with a 6° spread in starting latitude arrive within a 2° range. Even though such effects are observable in whistlers (compare the relative intensities of the WT and 1_- whistlers of Figure 2), they are particularly clear in the observations of fixed-frequency VLF transmissions. The fixed frequencies from 10.2 to 13.6 kHz transmitted by the Omega stations are in the range of frequencies observed in WT whistlers, and when received by a satellite in the hemisphere conjugate to the transmitter generally exhibit characteristics similar to those of the prevailing WT whistler activity. Several such effects, including focusing, are illustrated in Figure 10, which shows OGO 4 spectra received near 50° latitude in the southern hemisphere. Horizontal lines at the right end of the panels identify the signal frequencies 10.2, 11⅓, 12.4, and 12.5 kHz from the Omega transmitter in Forest Port, New York. In the top panel, the Omega signals appear as dashes of various lengths, and their intensity, as evidenced by the darkness of the display, drops sharply above and to the right of the sloping dark area that extends from ~51° to ~56°. In the expanded time-scale portions of this record marked *A* and *B* and shown in the middle and bottom panels, the dark area may be identified as having been produced by WT whistlers, in the form of somewhat irregular rising tones. Some contribution to the darkness of the record is made by relatively pure, falling-tone whistlers that accompany many of the WT events. The stronger signals from Omega are interpreted as the result of propagation in the WT mode, the intensity enhancement near 50° being associated with the focusing effect predicted in Figure 5*a* or Figure 6*b*. The weaker signals from Omega received at higher latitudes are believed to reach the satellite on paths similar to those of the 1_- whistlers marked by asterisks in Figure 1*a*.

The schedule of the transmitted pulses from Omega (Forest Port) is shown immediately above the middle and bottom panels in Figure 10. From a careful comparison of the transmitted and received pulses, it was found that the travel times of Omega signals increase rapidly with latitude, in agreement with the

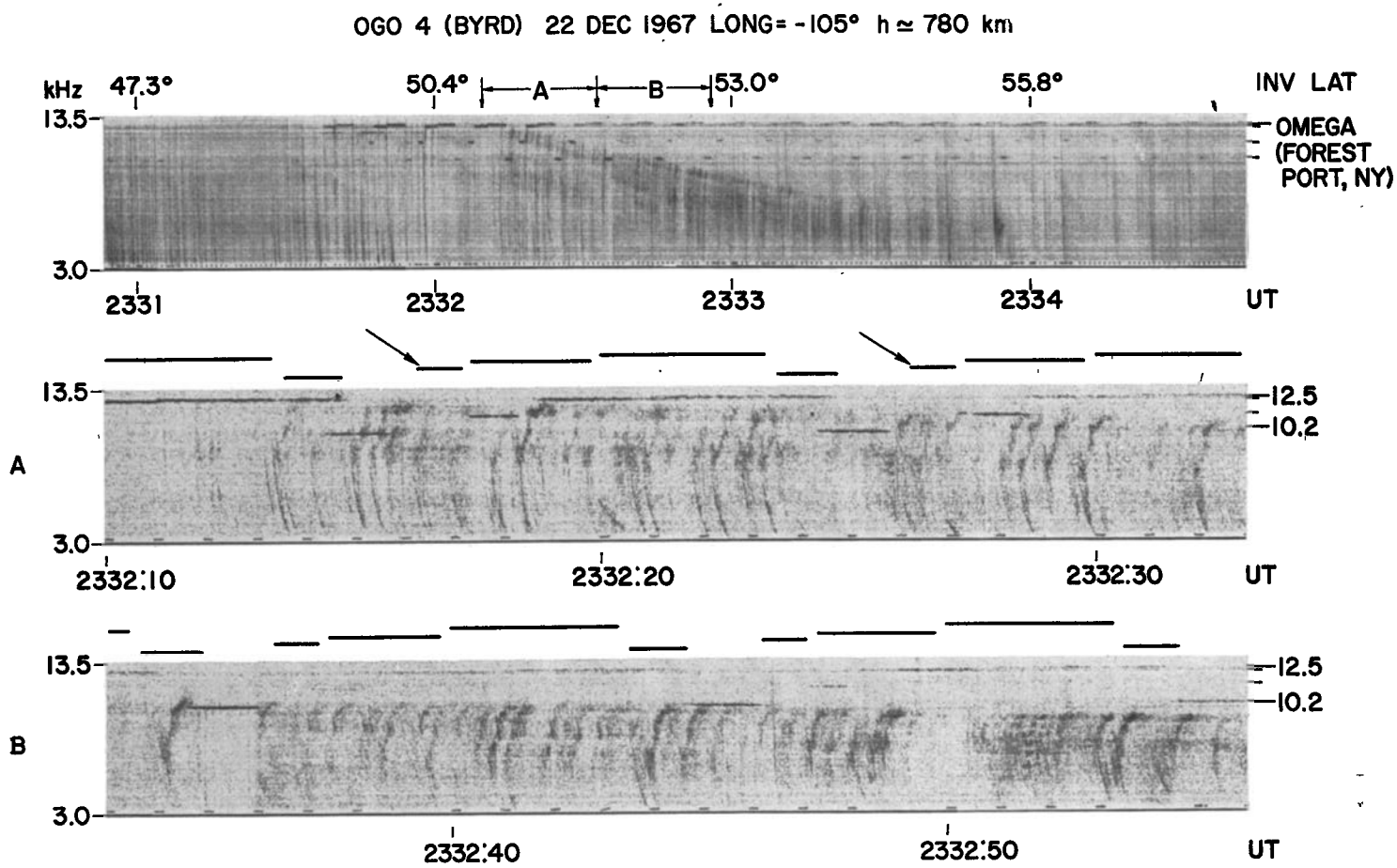

Fig. 10. Frequency-time spectrograms of VLF data received on OGO 4 near Byrd Station, Antarctica. The sloping dark portion near the center of the top panel is produced by whistlers. The horizontal dashes of variable lengths above 10 kHz are signals from Omega (Forest Port, New York) at 10.2, 11⅓, 12.4, and 12.5 kHz. The portions denoted *A* and *B* are presented with expanded time scale in the middle and bottom panels. Above these panels is the schedule of pulses transmitted from Omega, Forest Port, shown for comparison with the received signals (see text).

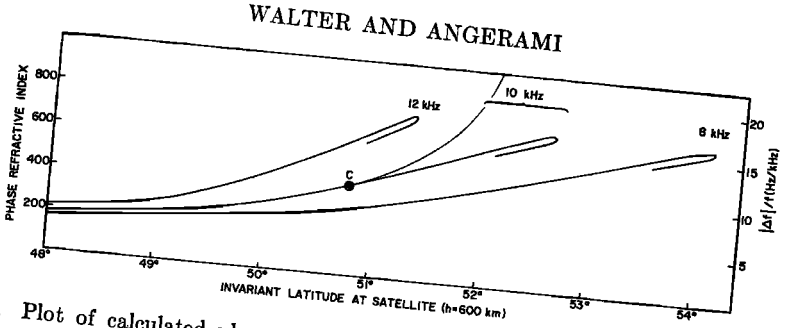

Fig. 11. Plot of calculated phase refractive index as a function of invariant latitude for three different frequencies. For illustration, point C corresponds to point B in Figure 6*a* and to path $A' - A$ in Figure 5*a*. The right-hand scale gives approximately the ratio between the expected Doppler shift (in Hz) and the wave frequency (in kHz), calculated for a satellite with velocity of 7.5 km/sec, assumed horizontal and in the magnetic meridian plane. The thin line represents calculations for the model with constant density at 1000 km shown in Figure 4.

predictions for the WT mode (cf. Figure 6*a*). This increase in travel time with latitude may be seen in panel A in the case of two pulses transmitted at 11⅓ kHz (arrows). The travel time from the trailing edge of the first transmitted pulse to the trailing edge of the corresponding received signal (below and just to the right) is ~1.1 sec. For the second pulse the time is increased to ~1.5 sec. The pulses received in the WT mode are longer than those transmitted, especially near the high-latitude cutoff. This is consistent with the behavior of the WT whistlers in the same figure, which on close inspection may be seen to exhibit pronounced increases in travel time with increasing frequency near the upper limiting frequency.

Doppler shift effects in the WT mode. The low phase velocities resulting from nearly transverse propagation at the end of the nonducted path (see Figure 5*a*) can cause a substantial Doppler shift when such waves are observed by a polar, low-altitude satellite such as OGO 4. Also, the Doppler shift can be positive or negative depending on whether the satellite is moving equatorward or poleward. The phase refractive indices calculated for three different frequencies are plotted as a function of invariant latitude in Figure 11, where point C corresponds to point B of Figure 6 (the thin line corresponds to the model of electron concentration constant at 1000 km (cf. Figure 4)). The relative Doppler shifts can be approximately obtained from the scale on the right, which was calculated taking the average velocity of OGO 4 to be 7.5 km sec^{-1}, horizontal, and in the magnetic meridian plane. The angle between the wave normal and the satellite velocity was taken as the complement of the average dip angle for the range of latitudes shown since, as already stated, the wave normal lies close to the normal to the magnetic field in this region. The plot predicts that the magnitude of the Doppler shift should increase both with frequency and latitude.

Clear evidence of Doppler and focusing effects in Omega signals has been found in records from twelve OGO 2 and OGO 4 passes. The Doppler shifts were negative in all but two cases, due to the poleward direction of satellite motion on most of the passes suitable for observing WT mode effects. (The number of such passes is limited by local-time restrictions on the distribution of electron concentration (described above), and by the requirement of approximate conjugacy to an Omega transmitter.)

Figure 12 shows examples from OGO 4 of Doppler shifts in WT mode signals from the Omega transmitter in Aldra, Norway. The transmission schedule of pulses of 10.2 and 11⅓ kHz is indicated in the upper margin. A negative shift (consistent in sign with the poleward direction of satellite motion) is particularly well illustrated by the first pair of signals near 11⅓ kHz (see Figure 3 for an expanded version of this part). The first weaker signal, corresponding to the 1- whistler of Figure 1*a*, exhibits no frequency shift. The second, WT-mode pulse, exhibits a clear negative offset of about 100 Hz and is visibly more intense than the other signal. A similar Doppler shift effect (~100

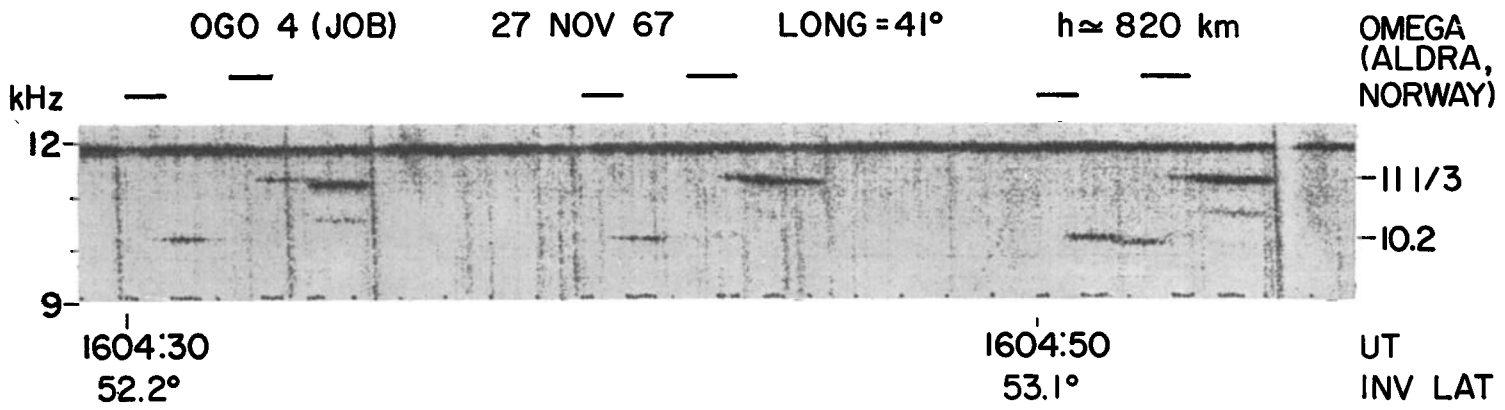

Fig. 12. OGO 4 frequency-time spectra received near Johannesburg, South Africa, illustrating Doppler shifts in signals form the Omega transmitter in Norway at 10.2 and 11⅓ kHz. The segments just above the spectrogram show the pattern of transmitted pulses. The first transmitted pulse at 11⅓ Hz produces two clearly distinct signals received at the satellite (an expanded record of this event is shown in Figure 3). The first signal is weaker and probably follows the same ducted path as most of the whistlers observed in this run (shown as nearly vertical traces). The segment with larger travel time is considerably stronger and propagates to the satellite in the WT mode, exhibiting a negative Doppler shift af about 100 Hz. A similar behavior is shown by the received signals produced by the last transmitted pulse at 10.2 kHz. The effect of flutter in the original tape recorder is apparent in the strong signal near 11.9 kHz (a transmission from an unidentified VLF transmitter).

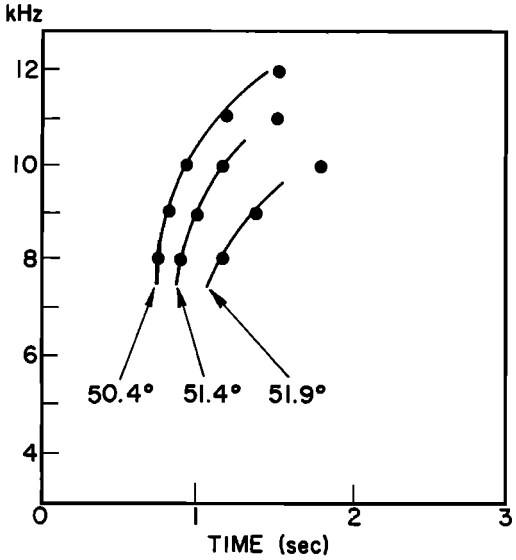

Fig. 13. Comparison of calculated and observed WT-whistler spectra. The continuous lines are transcriptions of frequency-time spectra of WT whistlers observed at the invariant latitudes indicated. The examples were taken from the events marked by heavy arrows in Figure 1*a*, the lightning source positions serving as a common time origin. Spectra of WT whistlers calculated for invariant latitudes corresponding to those of the observations are shown by dots.

Hz) is presented at higher latitudes by the pair of signals produced by the third transmitted pulse at 10.2 kHz. The two preceding signals at this frequency, received at lower latitudes, exhibit no detectable Doppler shift (less than 10 Hz), indicating that at this point the projection of the refractive index along the velocity of the satellite was less than ~50. Note that as the signal frequency is lowered, the latitude at which a given Doppler shift is observed increases, in agreement with the calculations plotted in Figure 11. This example (Figure 12) illustrates the confinement of WT-mode signals to a narrow range of latitudes, and their relatively high amplitudes.

A quantitative comparison between the Doppler shift calculated by ray tracing and the observations is not given here, for reasons explained in the later section on models of the earth's magnetic field.

Comparison between calculated and observed WT whistlers. The time-frequency spectra of the WT whistlers marked by heavy arrows in Figure 1*a* are shown by continuous lines in Figure 13 using the position of the lightning source (identified in Figure 1*a*) as a common time origin. The time-frequency spectra of WT whistlers calculated for the invariant latitudes and altitudes where the observations were made are shown by dots in the same figure. The calculations were made by tracing rays in the model magnetosphere already described, and from which Figure 6 was produced. There is evidently very close agreement in travel time between the observed and calculated spectra.

There is also excellent agreement between calculated and observed spectra on lower cutoff frequency. This was achieved by choosing a model density with a maximum LHR frequency above the satellite (Figure 7) equal to the lower cutoff frequency of the observed whistlers.

The upper cutoff frequencies for the calculated WT whistlers are somewhat higher than the ones shown by the data in Figure 13. At 51.4° invariant latitude for instance, Figure 6 predicts an upper cutoff of about 12 kHz, whereas the observed WT whistler extends only to 10.5 kHz (Figure 13). Several mechanisms have been considered to account for such a discrepancy.

One possibility is that rays traveling beyond $L = 3.0$ are Landau absorbed, since in this region the wave normals in the WT mode make large angles with the geomagnetic field (cf. Figure 5). (This type of interaction has been proposed to explain the absence of MR whistlers at high L shells [*Thorne*, 1968].) Before assessing the extent of this effect, it is necessary to examine the effect of horizontal gradients in the thermal plasma at low altitudes.

Another possibility is that an appropriate modification in the magnetospheric density model could lower the latitude of the upper cutoff shown in Figure 6*b* (nose of the solid curves). This hypothesis, which at present cannot be ruled out, involves further complications in the density model and is under study.

A third possible explanation of the discrepancy is that the plasmapause was located near $L = 3.0$ at the time of the observations. This would essentially invalidate the predictions of Figure 6 for the behavior of rays near the line $L_{max} = 3.0$. This possibility may be discarded, since at the time of the observations, the plasmasphere extended at least to $L = 3.7$. This

is shown by a plasmasphere level of equatorial density at $L = 3.7$ (dot in Figure 4) determined from nose whistlers received at OGO 4 within two minutes of the observations of the WT whistlers of Figure 1*a*.

5. Discussion

Earth's magnetic field model. Up to now rays have been traced in a two-dimensional magnetosphere where the earth's magnetic field is represented by a centered dipole. By tracing field lines in a magnetic field model given by *Cain et al.* [1968] it has been found that this field is well-represented by a centered dipole in the range of L values considered here and near the longitudes of Rosman (~97°W), but not near the longitudes of Johannesburg (~41°E), where the magnetic field lines are asymmetric. Under these conditions, it is not clear how to compare the results of ray tracings performed in a dipole field with observations near Johannesburg. A three-dimensional ray tracing in a magnetic field represented by a harmonic expansion [*Cain et al.*, 1968] was therefore developed (F. Walter, unpublished data, 1969) and used for a closer comparison with the data, using geographic coordinates.

Doppler shift results from the calculations using the two-dimensional (dipole field) and the three-dimensional ray tracing [*Cain et al.*, 1968] were compared for longitudes near Johannesburg (~41°E). It was found that the latitude at which a given Doppler shift (of ~100 Hz at 10 kHz) should be observed is about 1° lower for the dipole representation. Considering that the characteristics of signals propagating in the WT mode change very rapidly with latitude (note in Figure 1 the change in the spectra of WT whistlers observed in a range of 1.5° in latitude), one sees that a discrepancy of 1° is too large. As predicted, the magnetic field model has a first-order effect on the WT mode of propagation, and it is of little value to fit the data by changing density models only.

The electron concentration model. The electron concentration model used in the calculations of Figure 13 was developed on the basis of several independent sources of information. These included: (1) a value of equatorial electron concentration (shown as a dot at $L = 3.7$ in Figure 4) deduced from a whistler received at the satellite within two minutes of the observations illustrated in Figure 1*a*; and (2) an estimate of a maximum LHR frequency above the satellite of 7.4 kHz from the lower cutoff frequency of the WT whistler of Figure 1*a*. Successive approximations within the constraints of this evidence led to the diffusive equilibrium model described earlier and summarized (in terms of electron concentration) in Figure 4.

Another bit of evidence obtained since the calculations were made suggests that the model is representative of actual conditions prevailing in the magnetosphere at the time. This evidence, kindly provided by L. Colin of the NASA/Ames Research Center, Moffett Field, California, involves Alouette 2 topside sounder data obtained within 40 minutes and 30° longitude of the OGO 4 pass in question. The analysis showed an electron concentration of ~7500 el cm^{-3} at 1000 km and latitude 45°, in close agreement with the model used.

Related phenomena and further work in progress. Toward the higher latitudes a descending tone whose lower cutoff generally merges with the upper cutoff of the WT whistler is seen on occasion. The interpretation of this component is being studied in terms of inward leakage from the plasmapause and as a result of horizontal gradients in the ionosphere.

On several occasions, particularly during November 1967, artificially stimulated emissions (ASE) associated with Omega signals were observed on OGO 4. Some of the ASE's appear to be triggered by ducted signals, being in this respect similar to those observed on the ground (see *Carpenter et al.* [1969]), whereas some appear to be related to nonducted signals. The latter were observed both in the hemisphere conjugate to the transmitter and in the same hemisphere (in this case several echoes were also present). Study of the nonducted ASE's is in progress, using ray tracings to locate possible regions of generation and corresponding wave normal directions.

6. Summary and Conclusions

Evidence for nonducted whistler-mode propagation from one hemisphere to the conjugate ionosphere has been found in frequency-time spectra of VLF signals recorded by the broadband (0.3–12.5 kHz) receivers aboard the OGO 2 and OGO 4 polar satellites. The nonducted

TABLE 1

Predictions of Raytracing	Observations from OGO 4	Comments
(1) Large wave normal angles, with associated phase refractive index approaching 1000.	(1*a*) Doppler shifts up to several hundred Hz near 10 kHz.	
	(1*b*) Both positive and negative Doppler shifts, depending on equatorward or poleward motion of the satellite.	
(2) At a fixed frequency phase refractive index increases with latitude.	(2) At a fixed frequency, magnitude of Doppler shift increases with observing latitude.	
(3) At a fixed observing point, phase refractive index increases with frequency.	(3) At a fixed observing point, magnitude of Doppler shift increases with frequency.	
(4) For satellite below the level of the upper maximum in the LHR frequency, WT whistlers exhibit a single component with a low-frequency cutoff in intensity.	(4) Typical WT mode whistlers exhibit a single component with a lower cutoff (f_{lc0}) near 7 kHz.	(4) The OGO 4 orbit lies between ~500 and 900 km altitude. The observations imply the existence of a maximum in the LHR frequency above the satellite ($f_{lc0} \approx f_{\mathrm{LHR\,(max)}}$).
(5) For satellite above a maximum in the LHR frequency, WT whistlers exhibit two closely spaced components ($\Delta_t \approx 70$ msec).	(5) A small number of WT whistlers exhibit two closely spaced components with a lower cutoff (f_{lc0}) near 6 kHz and an upper cutoff of the reflected component (f_{uc0}) about 7 kHz.	(5) Implies the absence of a maximum in the LHR above the satellite. Implies that $f_{lc0} \approx f_{\mathrm{LHR\,(local)}}$ and $f_{\mathrm{LHR\,(max\ below\ satellite)}} \gtrsim f_{uc0}$.
(6) For satellite below the upper LHR maximum, the low frequency of WT whistlers is relatively constant with latitude.	(6) Over a typical observing range of 2–3° invariant, the lower cutoff frequency is usually constant within ~±5%.	(6) Implies that the upper maximum of the LHR frequency varies relatively slowly with latitude over the 2–3° observing range.
(7) At a fixed frequency, travel time increases with latitude.	(7) Observed in whistlers as the 'walking trace' effect, also observed in fixed frequency signals.	
(8) At a fixed observing point, travel time increases with frequency.	(8) Observed in both whistlers (rising tone) and fixed frequency signals.	
(9) A high-frequency cutoff in intensity.	(9) Observed in both whistlers and fixed frequency signals. In a case study the ray tracing predictions were about 1 kHz above the observed cutoffs (case of Figure 13).	(9) The discrepancy is possibly due to Landau damping or to effects of detailed features of the electron concentration distribution.
(10) Upper cutoff frequency decreases with latitude.	(10) Observed in both whistlers and fixed frequency signals. Frequency causes the WT mode to disappear as the upper cutoff reaches the relatively constant lower limiting frequency.	
(11) A high-latitude limit of observations near 55° invariant.	(11) WT mode observations thus far limited to latitudes <56° invariant.	
(12) Focusing effect (3 to 1 compression in latitude range at endpoint compared with input).	(12) Observed in whistlers, but particularly clearly in fixed frequency signals.	

TABLE 1 (*Continued*)

Predictions of Raytracing	Observations from OGO 4	Comments
(13) Well-defined WT-mode effects depend on a model ionosphere with relatively small horizontal gradients at 1000 km.	(13) Well-defined WT mode effects have not thus far been observed in daytime, when relatively large horizontal gradients exist in the latitude range of interest.	

propagation manifests itself both in naturally occurring whistlers and in man-made signals.

The whistlers have been called 'walking-trace' (WT) whistlers because their travel times increase rapidly with latitude, producing an effect of 'walking through' other whistler components that are excited by the same lightning sources but whose dispersion characteristics remain nearly unchanged with satellite position.

Many diverse characteristics of WT-mode propogation have been explained by ray tracings in a model magnetosphere represented by a dipole geomagnetic field and a diffusive-equilibrium distribution of ionization. Table 1 compares the results of ray tracing with the satellite observations. The excellent agreement obtained provides additional support for the ray tracing technique as a means of predicting the behavior of nonducted whistler-mode waves in the magnetosphere, and also suggests that the electron concentration field-line model used (diffusive equilibrium, with about 1200 el cm^{-3} at $L = 2.8$ at the equator) is a good approximation for the actual density in the plasmasphere.

Ray tracings in a geomagnetic field represented by a harmonic expansion were performed to explain the behavior of nonducted signals in regions near Johannesburg, South Africa, where the actual field departs substantially from a dipole representation. The latitudes at which a given Doppler shift is predicted using the dipole and the harmonic expansions were found to differ by 1°.

Applications. The diagnostic potential of the WT-mode remains to be fully evaluated. There are several promising possibilities, including use of WT whistlers to obtain information on (1) the plasma density and its gradient across the geomagnetic field in the magnetosphere, and on (2) the largest lower hybrid resonance (LHR) frequency above the satellite (from the lowest observed frequency), which in turn sets theoretical limits to ionic compositions.

WT whistlers presenting a double trace just above the lower cutoff indicate that the LHR frequency at the satellite is larger than all values above it. The condition imposes severe theoretical constraints on the rate at which the fractional abundance of H^+ can vary with altitude above the spacecraft.

Signals propagating in the WT mode at 10.2 and 11⅓ kHz from the U. S. Navy Omega stations have been observed in the conjugate hemisphere with amplitudes comparable to (or even larger than) those detected near the transmitter. The enhanced signal suggest the feasibility of communication between a low power VLF transmitter and a satellite in the conjugate region. For this application a better understanding of nonducted propagation is needed to cope with the Doppler shifts (up to hundreds of Hertz) that are normally present in the enhanced signals.

Acknowledgments. We wish to express our gratitude to Mr. J. Katsufrakis for calling attention to interesting data, to Prof. R. A. Helliwell and Dr. R. L. Smith for enlightening discussions, and to Dr. D. L. Carpenter for helpful criticism of the manuscript.

The research for this paper was supported in part by the National Aeronautics and Space Administration under contract NAS 5-3093 and grant NsG 174-SC/05-020-008; in part by the National Science Foundation, Office of Antarctic Programs under grants NSF GA 1151 and GA 1485; in part by the National Science Foundation, Office of Computer Sciences under grant NSF GP-948, and in part by the Office of Naval Research under contract ONR-N00014-67-A-0112, 0012. The work was carried out during the tenure of a scholarship awarded to one of the

authors (F. Walter) by Comissão Nacional de Atividades Espaciais (C. N. A. E.)—Brazil.

References

Angerami, J. J., and J. O. Thomas, Studies of planetary atmospheres, 1, The distribution of electrons and ions in the earth's ionosphere, *J. Geophys. Res., 69,* 4537, 1964.

Barrington, R. E., and J. S. Belrose, Preliminary results from Canada's Alouette satellite, *Nature, 198,* 651, 1963.

Brace, L. H., B. M. Reddy, and H. G. Mayr, Global behavior of the ionosphere at 1000-kilometer altitude, *J. Geophys. Res., 72,* 265, 1967.

Brice, N. M., and R. L. Smith, Lower hybrid resonance emissions, *J. Geophys. Res., 70,* 71, 1965.

Cain, J. C., S. Hendricks, W. E. Daniels, and D. C. Jensen, Computation of the main geomagnetic field from spherical harmonic expansion, *Data Unver's Note NSSDC 68-11, NASA/GSFC,* Greenbelt, Md., May 1968.

Carpenter, D. L., K. Stone, and S. Lasch, A case of artificial triggering of VLF magnetospheric noise during the drift of a whistler duct across magnetic shells, *J. Geophys. Res., 74,* 1848, 1969.

Haselgrove, J., Ray theory and a new method for ray tracing, *Rept. of Physical Society Conference on Physics of the Ionosphere,* 355, Cambridge, 1954.

Kimura, I., Effects of ions on whistler-mode ray tracing, *Radio Sci., 1,* 269, 1966.

Scarabucci, R. R., J. J. Angerami, and R. A. Helliwell, OGO-4 amplitude measurements of VLF signals—the pro-longitudinal whistler mode of propagation (in preparation), 1969.

Smith, R. L. and J. J. Angerami, Magnetospheric properties deduced from OGO 1 observations of ducted and nonducted whistlers, *J. Geophys. Res., 73,* 1, 1968.

Smith, R. L., I. Kimura, J. Vigneron, and J. Katsufrakis, Lower hybrid resonance noise and a new ionospheric duct, *J. Geophys. Res., 71,* 1925, 1966.

Storey, L. R. O., and J. C. Cerisier, Une interpretation des bandes de bruit au voisinage de la frequence hybride basse observees au moyen de satellites artificiels, *Compt. Rend., 266,* 525, 1966.

Thorne, R. M., Unducted whistler evidence for a secondary peak in the electron energy spectrum near 10 kev, *J. Geophys. Res., 73,* 4895, 1968.

Walter, F., Nonducted VLF propagation in the magnetosphere, *SU-SEL-69-061, Tech. Rept.,* Radioscience Lab., Stanford Electronics Labs., Stanford University, Stanford, Calif., 1969.

(Received July 28, 1969.)